

Revvng up ^{13}C NMR shielding predictions across chemical space: Benchmarks for atoms-in-molecules kernel machine learning with new data for 134 kilo molecules

Amit Gupta,¹ Sabyasachi Chakraborty,¹ and Raghunathan Ramakrishnan^{1, a)}

¹Tata Institute of Fundamental Research, Centre for Interdisciplinary Sciences, Hyderabad 500107, India

(Dated: 4 December 2020)

The requirement for accelerated and quantitatively accurate screening of nuclear magnetic resonance spectra across the small molecules chemical compound space is two-fold: (1) a robust ‘local’ machine learning (ML) strategy capturing the effect of neighbourhood on an atom’s ‘near-sighted’ property—chemical shielding; (2) an accurate reference dataset generated with a state-of-the-art first principles method for training. Herein we report the QM9-NMR dataset comprising isotropic shielding of over 0.8 million C atoms in 134k molecules of the QM9 dataset in gas and five common solvent phases. Using these data for training, we present benchmark results for the prediction transferability of kernel-ridge regression models with popular local descriptors. Our best model trained on 100k samples, accurately predict isotropic shielding of 50k ‘hold-out’ atoms with a mean error of less than 1.9 ppm. For rapid prediction of new query molecules, the models were trained on geometries from an inexpensive theory. Furthermore, by using a Δ -ML strategy, we quench the error below 1.4 ppm. Finally, we test the transferability on non-trivial benchmark sets that include benchmark molecules comprising 10 to 17 heavy atoms and drugs.

Keywords: NMR, Machine learning, Kernel ridge regression, Drug compounds

I. INTRODUCTION

Nuclear magnetic resonance (NMR) is an indispensable tool in chemistry, biochemistry and biophysics. It is fast, accurate, information-rich and non-destructive, making it the ideal technique for detecting or describing chemical bonding scenarios. As easy and trivial have most NMR experiments become, it is still a computationally expensive task to estimate NMR shielding tensors or coupling constants for large molecular datasets^{1,2}. While molecules with heavy atoms demand incorporation of relativistic corrections to achieve quantitative accuracy^{3,4}, computational NMR spectroscopy without such subtle effects are routinely used in organic chemistry^{5–11}. For a comprehensive review on computational NMR, refer to Ref. 12. Recently, Grimme *et al.*¹³ discussed the automated prediction of spin-spin coupled ^1H NMR in various solvents by accessing relevant conformers, to generate experimentally relevant NMR spectra, while Buevich *et al.*¹⁴ employed computer-assisted structure elucidation algorithms and predicted NMR results to analyse molecular geometries. Lauro *et al.*¹⁵ designed a protocol to identify stereoisomers using experimental and predicted NMR data.

Amongst many *ab initio* quantum chemistry frameworks^{16–20}, gauge-independent atomic orbital (GIAO)²¹ is the most popular. Within the GIAO framework, Cartesian components of the NMR shielding tensor, σ_{ij}^q , of a nucleus q is calculated as the

second-order magnetic response property^{22,23}

$$\sigma_{ij}^q = \frac{\partial^2 E}{\partial B_i \partial \mu_j^q}, \quad (1)$$

where E is the electronic energy of the molecule, B_i is a component of the external magnetic field, and μ_j^q is the j -th component of the magnetic moment of the nucleus q . The isotropic shielding is defined as one-third of shielding tensor’s trace, $\sigma_{\text{iso}} = (\sigma_{11} + \sigma_{22} + \sigma_{33})/3$. Comparison of predicted values of σ_{iso} with experimental results is done by calculating its ‘shift’ using a standard reference compound $\delta_{\text{iso}}^q = \sigma_{\text{iso}}^{\text{ref.}} - \sigma_{\text{iso}}^q$ ²⁴.

^1H and ^{13}C are amongst the most commonly studied NMR-active nuclei. Accurate *ab initio* computation of δ ^{13}C requires methods such as coupled-cluster singles doubles²⁵, or spin-component-scaled MP2 with a triple-zeta quality basis set to reach a mean error of < 1.5 ppm^{1,26}, albeit incurring a cost which prohibits the method’s applicability for high-throughput studies. Composite methods have been proposed—analogueous to the G_n thermochemistry methods²⁷—that exploit the additivity in basis set and correlation corrections to reach a greater accuracy^{25,28}. Another method involves tailoring exchange-correlation functionals of Kohn-Sham density functional approximations such as WC04 and WP04²⁹.

When relaxing the accuracy requirement—while retaining the generality—a density functional approach that has received wide attention, particularly for NMR calculations of both ^1H & ^{13}C nuclei, is mPW1PW91³⁰. This method has been shown to provide good results for acetals³¹, pyramidalized alkenes³², acetylenes, allenes, cumulenes^{33,34} and even natural products^{5,6}. The same

^{a)}Electronic mail: ramakrishnan@tifrh.res.in

approach has also been used to model the 2D-NMR spectrum of exo-2-norbornanecarbamic acid³⁵. Further, a multi-reference standard approach³⁶ has shown consistent estimations of chemical shifts in solutions with a triple-zeta basis set³⁷. Thus, even though Flaig *et al.*'s²⁶ benchmark study ranked the B97-2 functional high, next only to the MP2 method, the consistency of mPW1PW91 has motivated several works including a recent effort by Gerrard *et al.*³⁸, where the authors applied mPW1PW91 with the 6-311G(*d,p*) basis set to generate NMR chemical shielding and hetero-nuclear coupling constants of molecular components in experimentally characterized organic solids.

While direct application of DFT is feasible for any query molecule, the questions that arise in chemical compound space (CCS) explorations often concern property trends across large datasets, demanding realistically rapid evaluation of the desired property. To this end, machine learning (ML) based statistical inference, in combination with high-throughput *ab initio* computing, offers a viable alternative (see Ref. 39). This approach has received such widespread attention that a recent competition on the world-wide web, Kaggle, for ML-aided prediction of NMR spectra⁴⁰ saw a participation of 2,700 teams across the world. An earlier proof-of-concept study discussed the feasibility of exploiting the local behavior of NMR chemical shifts with ML to achieve transferability to systems that are larger than those used to train the model⁴¹. That work depended on a cut-off based local version of the Coulomb matrix (CM) descriptor⁴². Recently, Gao *et al.*⁴³ explored deep neural networks (DNNs) in their "DFT + ML" model and achieved mean-squares error of 2.10 ppm for ¹³C chemical shifts compared to experimental values. DNN has also been employed for modeling electronic spectra^{44–46}. Kernel-ridge regression (KRR) is another ML method offering accuracies comparable to that of DNN for spectroscopy applications^{47,48}. However, ML/deep learning may not be limited to single property applications when multiple properties can be explored^{44,49,50}.

As for descriptors, successive improvements have been made by projecting the three-dimensional molecular chemical structure into multidimensional tensors⁵¹, four-dimensional hyper-spherical harmonics⁵², or a continuous representation such as the variant smooth overlap of atomic positions—SOAP^{53,54}. The latter with Gaussian process regression⁵⁵ predicted chemical shifts with root-mean-squares-error (RMSE) of 0.5/4.3 ppm for ¹H/¹³C nuclei on 2k molecular solids, while with KRR it was successful in predicting ²⁹Si and ¹⁷O NMR shifts in glassy aluminosilicates across a wide temperature range⁵⁶ comparable to fragment-based estimations⁵⁷.

The joint descriptor-kernel formalism of Faber, Christensen, Huang, and Lilienfeld (FCHL) uses an integrated Gaussian kernel function accounting for three-body interactions in atomic environment yielding highly accurate results for global molecular properties such as atomization energies⁵⁸. Recently, FCHL-based KRR has been

applied to model ¹H, ¹³C shifts and *J*-coupling constants between these two nuclei for over 75k structures in the CSD³⁸. For a test set, which was not part of training, the same study noted mean absolute errors (MAE) of 0.23 ppm / 2.45 ppm / 0.87 Hz (RMSE: 0.35 ppm / 3.88 ppm / 1.39 Hz) for δ ¹H / δ ¹³C / ¹J_{CH}, respectively.

Here, we present gas and (implicit) solvent phase mPW1PW91/6-311+G(2*d,p*)-level chemical shielding for all atoms in the QM9 dataset⁵⁹ comprising 130,831 stable, synthetically feasible small organic molecules with up to 9 heavy atoms C, N, O and F—henceforth denoted the QM9-NMR dataset. We apply KRR-ML using training sets drawn from QM9-NMR, benchmark control settings, and rationalize their influence on the performance of large ML models using up to 100k training examples. It has been recently noted⁶⁰ that the Δ -ML approach⁶¹ facilitates better ML accuracies. Thus, with converged settings, we provide benchmark learning curves for ML and Δ -ML methods based on three local descriptors—CM, SOAP and FCHL. Finally, we evaluate the transferability of the local ML models—trained only on QM9 molecules—to larger systems in non-trivial benchmark sets that include several drug molecules, a small subset of GDB17⁶² with molecules comprising 10 to 17 heavy atoms and linear polycyclic aromatic hydrocarbons (PAHs).

II. METHODOLOGY

Among popular ML frameworks, KRR is one of the most consistent and accurate⁶³ framework. In KRR formalism, for a query entity (molecule or atom), *q*, a generic property *p* from a reference (experiment or theory), is estimated as a linear combination of radial basis functions (RBFs a.k.a. kernel functions)—each centered at one training entity. Values of these RBFs are calculated at *q*, then the distances between *q* and *N* training molecules defined via their descriptors **d** is given as

$$p^{\text{est}}(\mathbf{d}_q) = \sum_{t=1}^N c_t k(|\mathbf{d}_q - \mathbf{d}_t|). \quad (2)$$

The coefficients, *c_t*, one per training datum, are obtained through ridge-regression by minimizing the least-squares prediction error

$$\begin{aligned} \mathcal{L} &= \langle \mathbf{p}^{\text{ref}} - \mathbf{p}^{\text{est}} | \mathbf{p}^{\text{ref}} - \mathbf{p}^{\text{est}} \rangle + \lambda \langle \mathbf{c} | \mathbf{c} \rangle \\ &= \langle \mathbf{p}^{\text{ref}} - \mathbf{Kc} | \mathbf{p}^{\text{ref}} - \mathbf{Kc} \rangle + \lambda \langle \mathbf{c} | \mathbf{c} \rangle \end{aligned} \quad (3)$$

The size of the kernel matrix is *N* × *N*, each element defined in close analogy to the right side of Eq. 2, $K_{ij} = k(\|\mathbf{d}_i - \mathbf{d}_j\|)$, *i* and *j* going over *N* training elements, with $\|\cdot\|$ denoting a vector norm. Here, for the choice of CM and SOAP descriptors, we used the Laplacian kernel depending on an *L*₁ norm defined as $K_{ij} = \exp(-|\mathbf{d}_i - \mathbf{d}_j|/\omega)$, where ω defines the length scale of the exponential RBF. As shown in Ref. 64, optimal so-

lution to Eq. 3 amounts to solving the linear system

$$[\mathbf{K} + \lambda \mathbf{I}] \mathbf{c} = \mathbf{p}^{\text{ref}}. \quad (4)$$

The second term in the r.h.s. of Eq. 3 is apparent in Eq. 4; if the definition of the descriptor does not differentiate any two training entries, then \mathbf{K} becomes singular and a unique solution to Eq. 4 can only be found with a non-zero value for the regularization strength, λ . Both ω and λ constitute hyperparameters in the model, that require a cross-validated optimization before out-of-sample predictions. Any non-zero value of λ determined by cross-validation is an indication of the presence of redundant training entries, either due to data-duplication or poor quality of the descriptor. As shown in Ref. 65, in the absence of redundant training entries, λ can be set to zero and the learning problem translates to solving $\mathbf{K}\mathbf{c} = \mathbf{p}^{\text{ref}}$. Alternatively, when linear dependencies may be anticipated—due to numerically similar descriptor differences—rendering an off-diagonal element of \mathbf{K} to be ≈ 1 , a finite $\lambda = \epsilon$ may be used to shift the diagonal elements of \mathbf{K} away from 1.0 and the lowest eigenvalue away from 0.0 thereby aiding Cholesky decomposition.

Prior regularization, \mathbf{K} is a covariance or dispersion matrix with all of its off-diagonal elements bound strictly in the closed interval $[0, 1]$ with unit diagonal elements. As per Ref. 65, we can estimate ω independent of property by restricting K_{ij} corresponding to the largest descriptor difference, D_{ij}^{max} , to 0.5, as in

$$\omega_{\text{opt}}^{\text{max}} = D_{ij}^{\text{max}} / \log(2). \quad (5)$$

In the present study, we also explore the performances of the choices of ω based on D_{ij}^{mean} and D_{ij}^{median} that will differ from the value of ω_{opt} based on D_{ij}^{max} depending on the diversity of the training set descriptors

$$\omega_{\text{opt}}^{\text{mean}} = D_{ij}^{\text{mean}} / \log(2); \quad \omega_{\text{opt}}^{\text{median}} = D_{ij}^{\text{median}} / \log(2). \quad (6)$$

Later we show how these choices are in close agreement with ω_{opt} values found by a scan to minimize the error for a large hold out set. We also discuss how the kernel matrix constructed with $\omega_{\text{opt}}^{\text{median}}$ can be applied to model NMR shieldings from gas and different solvent phases.

The prediction error of an ML model can be unconditionally quenched with increasing training set size for a good choice of the descriptor; however, the exponential nature of the learning rate often necessitates an increase in the model’s size by orders of magnitude. While the resulting surge in the computational cost associated with the ML model’s execution speed is seldom prohibitive, training with examples of the order of 10^6 places too severe hardware restrictions. When such hardware limit is reached for training, further drop in an ML model’s error can be attained by training on the deviation of the property from inexpensive, yet qualitatively accurate baseline values in a Δ -ML fashion⁶¹.

$$\Delta p(\mathbf{d}_q^{\text{bas.}}) = p^{\text{tar.}}(\mathbf{d}_q^{\text{tar.}}) - p^{\text{bas.}}(\mathbf{d}_q^{\text{bas.}}) \quad (7)$$

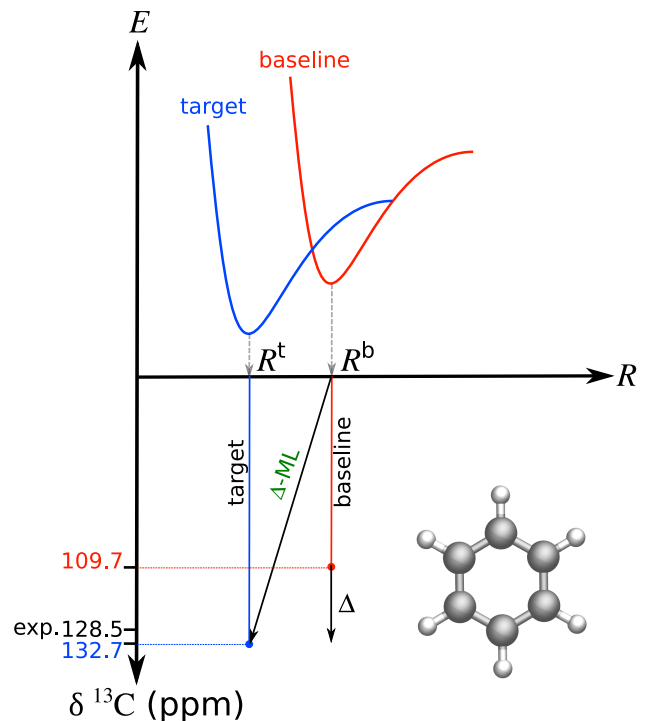


FIG. 1. Δ -ML of NMR chemical shifts exemplified by benzene; the model is trained to predict property from a target-level theory using as inputs atomic coordinates and the property from a baseline theory. The targetline and baseline shifts of benzene were computed at mPW1PW91/6-311+G(2d,p)@B3LYP/6-31G(2df,p) and B3LYP/STO-3G@PM7 levels, respectively.

The ML problem now involves solving for $\mathbf{K}\mathbf{c} = \Delta\mathbf{p}$. For any new prediction, Δ is augmented with the baseline

$$p^{\text{est.}}(\mathbf{d}_q^{\text{tar.}}) = p^{\text{bas.}}(\mathbf{d}_q^{\text{bas.}}) + \sum_{t=1}^N c_t k(|\mathbf{d}_q^{\text{bas.}} - \mathbf{d}_t^{\text{bas.}}|). \quad (8)$$

Fig. 1 illustrates Δ -ML for the modeling of NMR shifts with an example molecule. Often, for any given molecule, the determination of minimum energy geometry at the target level incurs a greater computational requirement than that is needed for the estimation of NMR shielding. In the Δ -ML framework, this problem can be alleviated by using atomic coordinates calculated at the same or a different baseline level for the construction of descriptors. Hence, new predictions can be rapidly made using structural information calculated at the baseline-level.

The formal requirements for a chemical descriptor have been discussed by others^{53,66–71}. Design of structure-based molecular descriptors drew inspiration from the success of generic coordinates such as atom-centered symmetry functions^{72,73}. Here, we explore CM⁴², SOAP^{53,54,74} and FCHL⁵⁸. For modeling local properties such as NMR shielding, CM can be truncated by a cutoff radius, r_{cut} ⁴¹, but there is always the possibility of failing to establish injective mapping between three di-

mensional molecular structure and the query property⁷⁵. Hence, more robust approaches include row-norm sorted CM or “bag of bonds”^{76–78}. Models based on all 3 descriptors show similar prediction times. For a detailed account of solver and prediction times on a single run, see Table. S2.

III. COMPUTATIONAL DETAILS

For training data in ML, we collected B3LYP/6-31G(2*df,p*)-level minimum energy geometries of 134k molecules in the QM9 dataset from Ref. 59. Those structures that have been reported to fragment during the geometry relaxation (3,054 in total) were excluded in this study. NMR shielding tensors of selected stable nuclei were calculated at the mPW1PW91/6-311+G(2*d,p*)-level in a single-point fashion within the GIAO framework^{79–81} using Gaussian-16 suite of programs⁸². In all DFT calculations, integration grid was set to `Ultrafine` with a `VeryTight` SCF threshold. To use as a baseline property in Δ -ML, we used NMR shielding calculated at the B3LYP/STO-3G level with geometries optimized at the PM7 level, the latter done with MOPAC⁸³. ¹³C isotropic shielding tensors, σ , were converted to ¹³C chemical shifts, δ , using a reference value for σ corresponding to that of tetramethylsilane (TMS), which was calculated in gas phase to be 186.97 ppm. We have also computed shielding tensors for the entire 131k set with implicit modeling of the solvents—carbon tetrachloride (CCl₄), tetrahydrofuran (THF), acetone, dimethyl sulfoxide (DMSO), and methanol—with the polarizable continuum model (PCM)⁸⁴. This was achieved by invoking `SCRF` in Gaussian-16 and specifying the solvent name and retaining default settings.

We have retained the same settings—mPW1PW91/6-311+G(2*d,p*)@B3LYP/6-31G(2*df,p*)—to calculate the NMR shielding of benchmark molecules that we selected for validating QM9-based ML models. Initial unrelaxed structures of the linear PAHs studied here have been taken from Ref. 85. From the GDB17 dataset, we have randomly selected 8 subsets of molecules, each with 25 molecules comprising 10–17 heavy atoms (200 in total). Further, we collected drug molecules present in the GDB17 dataset identified in Refs. 62, 86–88. In addition, we also collected 12 somewhat larger drug molecules from Ref. 89. The corresponding SMILES strings of all these ‘validation’ molecules, when available, were converted to initial Cartesian coordinates using the program `Openbabel`⁹⁰. Initial coordinates of the 12 large drug molecules were created using the `Avogadro`⁹¹ program. All molecules have been subjected to preliminary geometry relaxation performed with the force field `MMFF94`⁹². We used the default settings in `Dscribe`⁹³ and `QML`⁹⁴ to calculate the SOAP descriptor and the FCHL kernel matrix, respectively. All ML calculations have been performed using codes written in Fortran90 with interfaces to the `SCALAPACK`⁹⁵ numerical library.

IV. RESULTS AND DISCUSSIONS

A. QM9-NMR dataset

For a systematic exploration of NMR properties across the QM9 CCS, QM9-NMR dataset was created as per the procedures outlined in Section III. This dataset consists of data for stable 130,831 molecules amounting to 1,208,486 (1.3 M), 831,925 (832 k), 132,498 (132 k), 183,265 (183 k), 3,036 (3 k), NMR values for H, C, N, O, and F nuclei, respectively. DFT-level NMR shielding of these elements (Fig. 2a) demonstrate the expected range of values. In case of H, the most deshielded nucleus corresponds to the one from the cationic ammonium ion (encountered in zwitterionic molecules), while the most shielded proton belongs to a highly-strained secondary amine bonded to N. Methane offers the most shielded environment for ¹³C in QM9, whereas the most deshielded C features in a highly strained multiply-fused-ring molecule. Similarly, for N, the most shielded nuclei comes from a strained tertiary amine, whereas for O it features in a strained ring. Most deshielded N and O nuclei belong to a zwitterionic molecule.

Besides extrema, Fig. 2a also highlights the chemical diversity of the QM9 dataset. For C and H atoms, majority of the NMR shielding parameters come from C(*sp*³)-H bonds, indicating QM9 to largely comprise saturated organic molecules. Unsaturated molecules form a relatively smaller fraction of QM9 as can be seen in its shielding distribution function (between 0-75 ppm for C, Fig. 2b). N atom distribution shows two sharp distribution peaks at about 200 ppm and -35 ppm belonging to primary amine and cyano groups, respectively. Most frequent O atoms consist of ether linkages, while F atoms show a characteristic broad distribution around 250 ppm.

NMR shielding values for the entire dataset have also been calculated with continuum models of five commonly used polar and non-polar organic solvents: acetone, CCl₄, DMSO, methanol, and THF. Formally, a polar solvent will result in a more deshielded environment. However, the influence of the solvent is non-uniform across various C atoms in a molecule depending on the local environment of an atom in the molecule. Other effects such as hydrogen-bonding, halogen bonding may further influence the chemistry of the molecule resulting in unexpected chemical shifts. Thus, it is necessary to build a database comprising NMR shielding tensors calculated at various solvent media. Here as a first step, we computed the shielding values of the molecules in different solvents under a PCM framework. For a better description of the solvent environment it is essential to go beyond continuum modeling by using micro-solvation models that account for explicit solute-solvent interactions. The solvents were chosen to represent diverse environments: non-polar, polar aprotic and polar protic. For any given ¹³C nucleus, the spread in the shielding values due to the choice of the medium is at the most ± 4 ppm (Fig. S2) with minima and mean at 0 and 0.56 ppm,

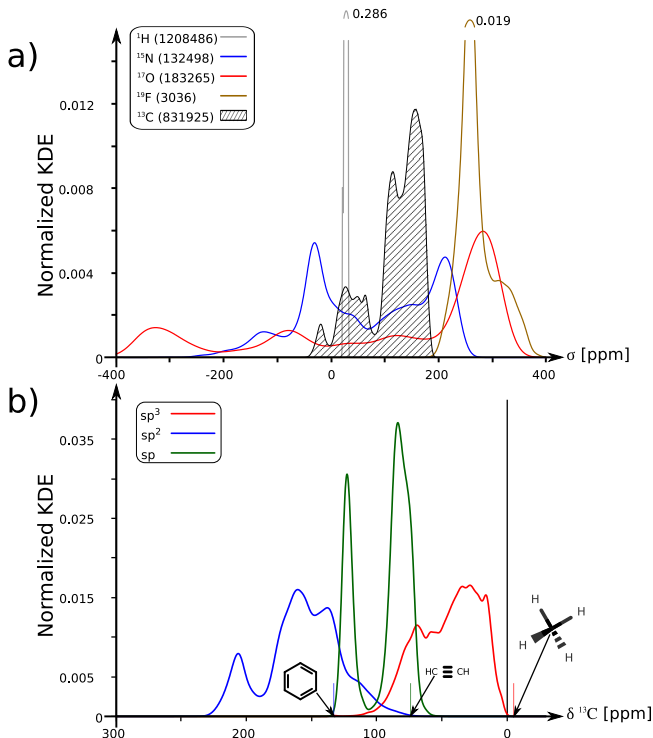


FIG. 2. Range of NMR shielding properties in the QM9-NMR dataset. a) Element-wise distribution of the shielding (σ in ppm) of all the nuclei in 131k QM9 molecules. b) ^{13}C chemical shifts (δ in ppm) for the QM9 molecules classified according to hybridization. KDE stands for kernel density estimation.

respectively, suggesting most nuclei to be minimally influenced by the implicit solvent environment. Hence, for ML predictions to differentiate the results from various phases, it is necessary that the models’ prediction accuracy is much less than ± 4 ppm.

QM9-NMR dataset also contains B3LYP/STO-3G NMR shielding constants for all the 130,831 molecules. Although the current ML study concerns itself with NMR shielding of the C-atom, the QM9-NMR dataset can be used to model other nuclei as well. To facilitate such and other *ab initio* benchmark efforts, the entire QM9-NMR dataset, comprising gas and solvent phase results, is now a part of the openly accessible MolDis big data analytics platform⁹⁶, <http://moldis.tifrh.res.in:3000/QM9NMR>.

B. AIM-ML modeling of NMR Shielding

Following the generation of the QM9-NMR dataset with 812k ^{13}C nuclei, we have selected a random set of 100k entries for training the ML models. Further, a separate subset of 50k nuclei—not overlapping with the 100k training entries—was kept for validating the ML models. Additionally, we have compared the distribution of the training and validation subsets with the total set, and found the normalized density distributions to be simi-

lar (Fig. S1). Therefore, we believe that the ML models based on large training sets presented here do not suffer from a selection bias.

All hyperparameters employed in the ML models have been optimized via cross validation within the training set. Through a logarithmic grid search, a value of 10^{-3} for λ was considered appropriate, and was kept constant throughout. NMR shifts are a local property, i.e., for any given atom, only neighboring atoms within a certain ‘sphere of influence’ contribute towards the chemical shift. Hence, the effective radius of such sphere, r_{cut} , has to be determined empirically. Fig. S3 lists the prediction errors for different descriptors at various cutoff values, in gas and solvent phases. It highlights one clear distinguishing feature between CM/SOAP descriptors, and FCHL; as the cutoff is increased to include more information in the kernel, CM’s and SOAP’s accuracies show best performances at about 2.3 and 2.0 Å respectively, beyond which the accuracy drops. FCHL, on the other hand, due to the presence of higher-order damping terms, shows a convergent behaviour with the accuracy saturating at 4.0 Å.

The kernel width, ω , was chosen separately for each descriptor; optimal value of this parameter for a given descriptor is inherently coupled to the dimensionality, completeness and the metric of the “feature spaces”. As the numerical values of the descriptor differences need not be same across descriptor definitions (Fig. S6), a single ω cannot scale two different kernels with same efficiency. This fact also sheds light on a heuristic approach for determining ω —from the descriptor differences, D_{ij} , independent of the property being modeled. We have tested the performance of optimal ω derived using Eq. 6 and found the values derived using the median of $\{D_{ij}\}$ to perform better than those based on the maximal (Eq. 5) or mean values (Eq. 6) (Table S1). For CM and SOAP descriptors, we found these values to be 422.78 and 18.85, respectively that we have adapted throughout this study. For these two choices of descriptors, we have also performed a cross validation to find out the best values of ω coinciding with $\omega_{\text{opt}}^{\text{median}}$ (vertical lines in Fig. S4). Due to the fact that the FCHL implementation in QML does not provide D_{ij} values, a grid search showed the best ω to be 0.3 (Fig. S5). Fig. S7 features the distribution of the kernel matrix elements based on 10k training examples for all three descriptors. While the distributions for CM and SOAP are rather univariate, FCHL’s K_{ij} values show a multivariate distribution, implying the latter model to be sensitive to the choice of the kernel width.

After determining the most appropriate hyperparameters for various choices of descriptors, we collected 10 training sets of sizes: 100, 200, 500, 1k, 2k, 5k, 10k, 20k, 50k, and 100k. We ensured that each smaller dataset is a subset of a larger one making the learning monotonous. We solved the linear equations of ML (Eq. 4) using Cholesky decomposition, and the trained machine was used to predict NMR shifts of 50k out-of-sample validation set. Mean absolute error (in ppm) for these 50k

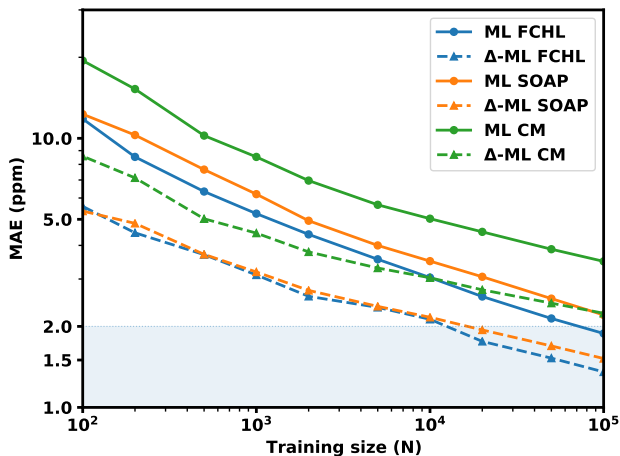


FIG. 3. ML and Δ -ML out-of-sample prediction errors for CM, SOAP and FCHL descriptors. For increasing trainingset size, N , mean absolute error (MAE) in the prediction of NMR shielding of 50k hold-out ^{13}C atoms are shown.

predictions was admitted as the sole performance metric of the training accuracy (Fig. 3). It also shows the performances of Δ -ML carried out using B3LYP/STO-3G NMR parameters at PM7 structures.

Overall, one notes from Fig. 3 that for all descriptors Δ -ML models converging by more than an order of magnitude faster (in terms of training set size) than direct ML ones. It is also evident that among all three descriptors, FCHL delivers the best performance with an average prediction error of < 2 ppm; the error drops below 1.4 ppm for Δ -ML modeling. However, it may be noted that for training set sizes $\leq 10\text{k}$, both FCHL and SOAP-based Δ -ML models yielded identical predictions, with SOAP showing an exponential learning rate, while FCHL showing a slightly faster rate going from 10k to 20k training examples—both Δ -ML models delivering ≈ 2 ppm accuracy already for 20k training. The similarity in performance between SOAP and FCHL can be observed in Fig. S10 both yielding similar correlation-coefficient across the training set in both ML and Δ -ML. For all case-studies, we used FCHL-100k ML and Δ -ML machines.

The origin of accuracy limiting factors in ML was further investigated by categorizing errors based on the NMR shielding range and the representation of the categorized region in the training dataset (Fig. S9). We found that the errors were not uniformly distributed and for certain shielding constant ranges, mean and variance of predictions were more erratic. The anomalous error in the -25 to 25 ppm region can be explained by i) under-representation of the aromatic or unsaturated systems in QM9, and ii) larger chemical diversity in the shifts of the unsaturated regions. In the 150–175 ppm region, where we found majority of C shielding values of the QM9-NMR dataset to lie, the prediction errors were rather low and less spread out. We note that as more data is added in

the erroneous regions (such as the -25 to 25 ppm region), the accuracy of the NMR machine improves.

We also probed if the baseline ^{13}C shielding values computed in gas phase can be utilized also for modeling DFT-level values in various solvents. While it is possible to simultaneously model on multiple property vectors by feeding in a rectangular matrix—row of column vectors—to the Cholesky procedure, the cost of training can be slightly minimized by inverting the kernel matrix once and multiplied with any arbitrary property vector to get new training coefficients⁶⁵. Table I demonstrates the versatility of this approach. Inverted FCHL-100k kernel instantly yielded trained machines for all solvents, with sub 2 ppm accuracy. From gas phase to DMSO ($\epsilon = 46.8$), we note a modest deterioration in performance.

TABLE I. Prediction errors of FCHL-based ML and Δ -ML models, with 100k training examples, in different media. Mean absolute errors in the prediction of the NMR shielding of 50k hold-out ^{13}C atoms are reported in ppm.

Medium (ϵ)	ML	Δ -ML
Gas	1.88	1.36
CCl_4 (2.228)	1.91	1.38
THF (7.426)	1.99	1.48
Acetone (20.493)	1.93	1.42
Methanol (32.613)	1.94	1.42
DMSO (46.826)	1.99	1.49

C. Application of FCHL-based ML & Δ -ML models

The magnitude of NMR chemical shift/shielding of a ^{13}C nucleus in a molecule is governed by its local environment. The inherent locality of this property implicitly suggests the shielding effect to drop with increasing distance. Subsequently, the information gained from a local moiety of a small test molecule can be reasonably transferred to the same local environment in a large molecule, provided the moiety is not perturbed by chemical interactions alien to the training molecule.

Using the 100k ML and Δ -ML machines, we investigate how well these properties can be estimated for larger molecules. The graph-based design of the GDB datasets allows one to explore CCS in an unbiased fashion. In Fig. 4, we explore our ML and Δ -ML models’ performances across GDB n datasets (where $n = 10, 11, \dots, 17$) using 25 randomly chosen molecules per n . Each of these 200 molecules were relaxed at the B3LYP/6-31G(2df,p) level with reference NMR shielding tensors calculated at the mPW1PW91/6-311+G(2d,p) level (Section III).

As expected, Δ -ML generally improves upon ML consistently yielding lower MAE and RMSD. Further, we note maximum average error per molecule (MAX) to overall improve with Δ -ML except for GDB15 and GDB11 possibly due to systems with interactions alien to GDB9. In Fig. 4, ML provides an MAE of < 4 ppm

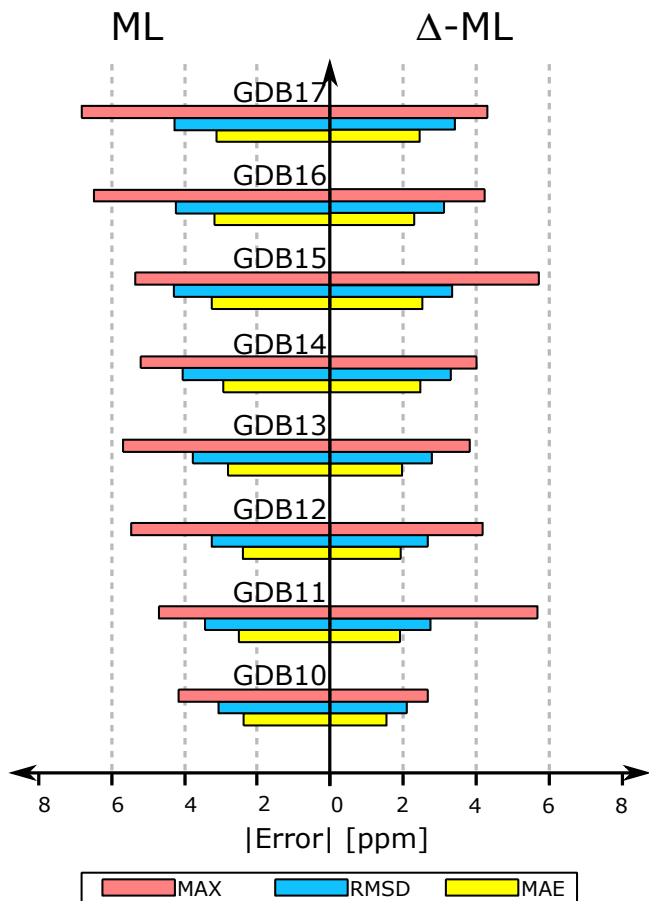


FIG. 4. Error metrics for ML and Δ -ML predictions of mPW1PW91/6-311+G(2*d*,*p*)-level ^{13}C chemical shifts of randomly chosen 25 molecules with n heavy atoms from the GDB*n* subsets of GDB17; $n = 10, \dots, 17$. MAE, RMSD and MAX correspond to mean absolute error, root-mean-squares-deviation and maximal error after averaging over all C atoms in a molecule, respectively.

across the datasets while it is usually below 3 ppm for Δ -ML. Arguably, 25 random molecules is not an accurate representation of the entire dataset in question and hence trends intrinsic to these subsets are not transferable across sets. Still, a general observation can be made: increasing number of heavy atoms introduces long-range influences on moieties rendering our machines somewhat inefficient—MAE of both ML and Δ -ML generally increase as we explore larger systems. Thus, apart from small fluctuation in the error trend across GDB10-GDB17—possibly due to sampling bias—the local models trained on GDB9 provide quantitative prediction for molecules larger than those used in training.

GDB*n* universe contains many drug molecules^{62,86–88}. Fig. S11 displays 40 such molecules. We tested our models’ efficiency in predicting ^{13}C NMR shielding values, and present their error metrics across direct and Δ -ML machines for each molecule. As Spearman coefficients are sensitive to numerical precision, we utilized a modi-

fied version by mapping the stick spectrum of the NMR shielding by a step function of height 1 and width of 1 ppm, when needed. The largest Δ -ML error encountered in this set is for Desflurane due to the presence of di- and tri-fluoro methyl groups that are under-represented in the training set. The second largest Δ -ML error is for Diethylcarbamazine stemming from deficiencies in baseline data. We note a total of 25 and 5 systems to show MAE higher than 3.0 ppm in ML and Δ -ML modeling, respectively. Barring 6 systems, Δ -ML improves upon direct ML’s MAE, a trend previously noted in Fig. 3 and Fig. 4; not only does it improve MAE, but for 14 systems it also improves ρ . Evidently, Δ -ML modeling helps to reach semi-quantitative predictions due to the accuracy of the baseline. In Fig. S12, we present 12 extra-GDB drugs with their error metrics and DFT chemical shifts. As expected, Δ -ML outperforms direct-ML consistently across all 12 molecules. The highest deviation is noted for Morphine with Δ -ML presenting an MAE > 3.0 ppm possibly because of moieties under-represented in QM9. However, for others the inherent locality of NMR shifts aid prediction. Drugs with extended delocalization present errors, since conjugation is inadequately captured in our ML-models. This deficiency is further noted in Fig. S13 where predicted chemical shifts of interstitial atoms of PAHs show the maximum deviation.

V. CONCLUSION

We present the QM9-NMR dataset that augments the QM9 set⁵⁹—containing DFT-level structures and properties of 134k organic molecules—with NMR shielding values computed at the mPW1PW91/6-311+G(2*d*,*p*)-level for about 2.4 million atoms constituting the molecules in this dataset. It may be further extended by including J -coupling between ^1H and other nuclei so that the diverse array of nuclei and properties present in QM9-NMR may aid seamless data-mining or ML studies. The impressive size of the dataset compelled us to explore solvent-phase values using an implicit solvation model, which however may not be adequate to describe effects due to the solute-solvent explicit interactions as addressed in Ref. 97. We focus on predicting the isotropic shielding values of ^{13}C nuclei in QM9 entries through KRR-ML models with Laplacian kernels. Upon benchmarking the performance of ML models across 3 descriptors: CM, SOAP and FCHL, we note a monotonous improvement in learning with increasing training set size up to 100k, with respect to predictions for a 50k hold-out set, where an FCHL-based (without alchemical corrections) ML-model showed the least MAE of 1.88 ppm. Δ -ML, using PM7 geometries and B3LYP/STO-3G baseline values, improves upon this accuracy to yield an MAE of 1.36 ppm. This is an improvement over the current record in out-of-sample prediction error in data-driven ^{13}C nuclei NMR shielding modeling³⁸. SOAP-based ML model’s under-performance could be speculated to the

use of Laplacian kernel-based KRR when Gaussian process regression is more effective. The performance drops with increasing diversity of validation molecules but the target being of local nature benefits from our models and aids in the prediction of ^{13}C shielding in molecules much larger than those in training set. Such a trend has been noted during the validation of ^{13}C shielding for a random subset of 25 molecules collected from GDB10 to GDB17 sets. Although, the prediction accuracy decreased with increasing molecular sizes, the MAE reported across datasets remained within 4.0 ppm for ML and 3.0 ppm for Δ -ML. When predicting ^{13}C shielding of drug molecules—one containing 40 drug molecules from GDB17 universe (Fig. S11), and the other containing 12 drugs with 17 or more heavy atoms (Fig. S12)— Δ -ML improves upon ML’s performance with the MAE decreasing from 3.7/4.2 ppm to 2.3/2.6 ppm for 40-drug/12-drug datasets, respectively. However, delocalization in linear PAHs (Fig. S13) proves challenging because of the small cutoff values decided from cross validation on molecules lacking such effects.

While the deficiency in our models should not fade with other local descriptors⁹⁸, augmenting the training set with systems displaying extended conjugation such as PAHs, fullerenes etc., or improving upon the current baseline for Δ -ML should lead to better accuracies. This opens exciting possibilities of ML-guided analysis into nucleus independent chemical shifts complimenting the latest tight-binding model for PAHs⁹⁹. Although our 100k training set is an adequate representation of the QM9 dataset, adaptive sampling method employed in Ref. 38 might be useful when using smaller training sets. Given the locality of the shielding property, it may be helpful to employ different machines⁴⁷ trained on *sp*, *sp*² and *sp*³ C—to account for systematic deviations in each groups. Finally, one can always improve the QM9-NMR dataset by estimating the effects from geometries obtained at ω B97XD with triple-zeta quality basis set.

VI. ACKNOWLEDGMENTS

The authors thank Vipin Agarwal, Kaustubh R. Mote and O. Anatole von Lilienfeld for fruitful discussions. This project was funded by intramural funds at TIFR Hyderabad from the Department of Atomic Energy (DAE). All calculations have been performed using the Helios computer cluster, which is an integral part of the MolDis Big Data facility, TIFR Hyderabad (<https://moldis.tifrh.res.in/>).

VII. DATA AVAILABILITY

The data that support the findings of this study are openly available in the MolDis repository, <http://moldis.tifrh.res.in:3000/QM9NMR>. For further details see supplementary information.

REFERENCES

- 1 T. Helgaker, M. Jaszuński, and K. Ruud, *Chem. Rev.* **99**, 293 (1999).
- 2 F. A. Mulder and M. Filatov, *Chem. Soc. Rev.* **39**, 578 (2010).
- 3 A. Bagno, F. Rastrelli, and G. Saielli, *J. Phys. Chem. A* **107**, 9964 (2003).
- 4 J. Novotny, M. Sojka, S. Komorovsky, M. Necas, and R. Marek, *J. Am. Chem. Soc.* **138**, 8432 (2016).
- 5 G. Bifulco, L. Gomez-Paloma, and R. Riccio, *Tetrahedron Lett.* **44**, 7137 (2003).
- 6 P. Cimino, L. Gomez-Paloma, D. Duca, R. Riccio, and G. Bifulco, *Magn. Reson. Chem.* **42**, S26 (2004).
- 7 I. D. Seymour, D. S. Middlemiss, D. M. Halat, N. M. Trease, A. J. Pell, and C. P. Grey, *J. Am. Chem. Soc.* **138**, 9405 (2016).
- 8 T. Bamine, E. Boivin, F. Boucher, R. J. Messinger, E. Salager, M. Deschamps, C. Masquelier, L. Croguennec, M. Ménétrier, and D. Carlier, *J. Phys. Chem. C* **121**, 3219 (2017).
- 9 S. Molchanov, T. Rowicki, A. Gryff-Keller, and W. Koźmiński, *J. Phys. Chem. A* **122**, 7832 (2018).
- 10 R. N. Guzzo, M. J. C. Rezende, V. Kartnaller, J. W. d. M. Carneiro, S. R. Stoyanov, and L. M. da Costa, *J. Mol. Struct.* **1157**, 97 (2018).
- 11 A. M. Sarotti, *Org. Biomol. Chem.* **16**, 944 (2018).
- 12 M. W. Lodewyk, M. R. Siebert, and D. J. Tantillo, *Chem. Rev.* **112**, 1839 (2012).
- 13 S. Grimme, C. Bannwarth, S. Dohm, A. Hansen, J. Pisarek, P. Pracht, J. Seibert, and F. Neese, *Angew. Chem. Int. Ed.* **56**, 14763 (2017).
- 14 A. V. Buevich and M. E. Elyashberg, *Magn. Reson. Chem.* **56**, 493 (2018).
- 15 G. Lauro, P. Das, R. Riccio, D. S. Reddy, and G. Bifulco, *J. Org. Chem.* **85**, 3297 (2020).
- 16 T. A. Keith and R. F. Bader, *Chem. Phys. Lett.* **194**, 1 (1992).
- 17 T. A. Keith and R. F. Bader, *Chem. Phys. Lett.* **210**, 223 (1993).
- 18 F. Mauri, B. G. Pfrommer, and S. G. Louie, *Phys. Rev. Lett.* **77**, 5300 (1996).
- 19 T. Gregor, F. Mauri, and R. Car, *J. Chem. Phys.* **111**, 1815 (1999).
- 20 W. Kutzelnigg, U. Fleischer, and M. Schindler, in *Deuterium and shift calculation* (Springer, 1990) pp. 165–262.
- 21 R. Ditchfield, *J. Chem. Phys.* **56**, 5688 (1972).
- 22 A. Hincliffe, *Ab initio Determination of Molecular Properties* (A. Hilger, 1987).
- 23 J. Gauss, *Modern Methods and Algorithms of Quantum Chemistry* **3**, 541 (2000).
- 24 M. Mehring, *High Resolution NMR Spectroscopy in Solids*, NMR Basic Principles and Progress (Springer Berlin Heidelberg, 2012).
- 25 D. R. Price and J. F. Stanton, *Org. Lett.* **4**, 2809 (2002).
- 26 D. Flaig, M. Maurer, M. Hanni, K. Braunger, L. Kick, M. Thubauville, and C. Ochsenfeld, *J. Chem. Theory Comput.* **10**, 572 (2014).
- 27 L. A. Curtiss, P. C. Redfern, and K. Raghavachari, *Wiley Interdiscip. Rev. Comput. Mol. Sci.* **1**, 810 (2011).
- 28 V. A. Semenov, D. O. Samultsev, and L. B. Krivdin, *J. Phys. Chem. A* **123**, 8417 (2019).
- 29 K. W. Wiitala, T. R. Hoye, and C. J. Cramer, *J. Chem. Theory Comput.* **2**, 1085 (2006).
- 30 C. Adamo and V. Barone, *J. Chem. Phys.* **108**, 664 (1998).
- 31 W. Migda and B. Rys, *Magn. Reson. Chem.* **42**, 459 (2004).
- 32 S. Vázquez, *J. Chem. Soc., Perkin Trans. 2*, 2100 (2002).
- 33 K. B. Wiberg, J. D. Hammer, K. W. Zilm, and J. R. Cheeseman, *J. Org. Chem.* **64**, 6394 (1999).
- 34 K. B. Wiberg, J. D. Hammer, K. W. Zilm, T. A. Keith, J. R. Cheeseman, and J. C. Duchamp, *J. Org. Chem.* **69**, 1086 (2004).
- 35 C. Bassarello, P. Cimino, L. Gomez-Paloma, R. Riccio, and G. Bifulco, *Tetrahedron* **59**, 9555 (2003).
- 36 A. M. Sarotti and S. C. Pellegrinet, *J. Org. Chem.* **74**, 7254 (2009).

- ³⁷A. M. Sarotti and S. C. Pellegrinet, *J. Org. Chem.* **77**, 6059 (2012).
- ³⁸W. Gerrard, L. A. Bratholm, M. J. Packer, A. J. Mulholland, D. R. Glowacki, and C. P. Butts, *Chem. Sci.* **11**, 508 (2020).
- ³⁹C. Cobas, *Magn. Reson. Chem.* (2020).
- ⁴⁰L. A. Bratholm, W. Gerrard, B. Anderson, S. Bai, S. Choi, L. Dang, P. Hanchar, A. Howard, G. Huard, S. Kim, *et al.*, arXiv preprint arXiv:2008.05994 (2020).
- ⁴¹M. Rupp, R. Ramakrishnan, and O. A. von Lilienfeld, *J. Phys. Chem. Lett.* **6**, 3309 (2015).
- ⁴²M. Rupp, A. Tkatchenko, K.-R. Müller, and O. A. von Lilienfeld, *Phys. Rev. Lett.* **108**, 058301 (2012).
- ⁴³P. Gao, J. Zhang, Q. Peng, J. Zhang, and V.-A. Glezakou, *J. Chem. Inf. Model.* (2020).
- ⁴⁴K. Ghosh, A. Stuke, M. Todorović, P. B. Jørgensen, M. N. Schmidt, A. Vehtari, and P. Rinke, *Adv. Sci.* **6**, 1801367 (2019).
- ⁴⁵J. Westermayr and P. Marquetand, *J. Chem. Phys.* **153**, 154112 (2020).
- ⁴⁶C. D. Rankine, M. M. Madkhali, and T. J. Penfold, *J. Phys. Chem. A* (2020).
- ⁴⁷R. Ramakrishnan, M. Hartmann, E. Tapavicza, and O. A. von Lilienfeld, *J. Chem. Phys.* **143**, 084111 (2015).
- ⁴⁸B.-X. Xue, M. Barbatti, and P. O. Dral, *J. Phys. Chem. A* **124**, 7199 (2020).
- ⁴⁹J. Westermayr, F. A. Faber, A. S. Christensen, O. A. von Lilienfeld, and P. Marquetand, *Mach. Learn.: Sci. and Technol.* **1**, 025009 (2020).
- ⁵⁰W. Pronobis, K. T. Schütt, A. Tkatchenko, and K.-R. Müller, *Eur. Phys. J. B* **91**, 178 (2018).
- ⁵¹H. Huo and M. Rupp, arXiv preprint arXiv:1704.06439 **13754** (2017).
- ⁵²A. P. Bartók, M. C. Payne, R. Kondor, and G. Csányi, *Phys. Rev. Lett.* **104**, 136403 (2010).
- ⁵³A. P. Bartók, R. Kondor, and G. Csányi, *Phys. Rev. B* **87**, 184115 (2013).
- ⁵⁴S. De, A. P. Bartók, G. Csányi, and M. Ceriotti, *Phys. Chem. Chem. Phys.* **18**, 13754 (2016).
- ⁵⁵F. M. Paruzzo, A. Hofstetter, F. Musil, S. De, M. Ceriotti, and L. Emsley, *Nat. Commun.* **9**, 1 (2018).
- ⁵⁶Z. Chaker, M. Salanne, J.-M. Delaye, and T. Charpentier, *Phys. Chem. Chem. Phys.* **21**, 21709 (2019).
- ⁵⁷J. D. Hartman, R. A. Kudla, G. M. Day, L. J. Mueller, and G. J. Beran, *Phys. Chem. Chem. Phys.* **18**, 21686 (2016).
- ⁵⁸F. A. Faber, A. S. Christensen, B. Huang, and O. A. von Lilienfeld, *J. Chem. Phys.* **148**, 241717 (2018).
- ⁵⁹R. Ramakrishnan, P. O. Dral, M. Rupp, and O. A. von Lilienfeld, *Sci. Data* **1**, 140022 (2014).
- ⁶⁰P. O. Dral, A. Owens, A. Dral, and G. Csányi, *J. Chem. Phys.* **152**, 204110 (2020).
- ⁶¹R. Ramakrishnan, P. O. Dral, M. Rupp, and O. A. von Lilienfeld, *J. Chem. Theory Comput.* **11**, 2087 (2015).
- ⁶²L. Ruddigkeit, R. Van Deursen, L. C. Blum, and J.-L. Reymond, *J. Chem. Inf. Model.* **52**, 2864 (2012).
- ⁶³F. A. Faber, L. Hutchison, B. Huang, J. Gilmer, S. S. Schoenholz, G. E. Dahl, O. Vinyals, S. Kearnes, P. F. Riley, and O. A. von Lilienfeld, *J. Chem. Theory Comput.* **13**, 5255 (2017).
- ⁶⁴R. Ramakrishnan and O. A. von Lilienfeld, *Rev. Comput. Chem.* **30**, 225 (2017).
- ⁶⁵R. Ramakrishnan and O. A. von Lilienfeld, *CHIMIA* **69**, 182 (2015).
- ⁶⁶A. Mauri, V. Consonni, and R. Todeschini, "Molecular descriptors," in *Handbook of Computational Chemistry*, edited by J. Leszczynski, A. Kaczmarek-Kedziera, T. Puzyn, M. G. Papadopoulos, H. Reis, and M. K. Shukla (Springer International Publishing, Cham, 2017) pp. 2065–2093.
- ⁶⁷M. Randić, *J. Math. Chem.* **19**, 375 (1996).
- ⁶⁸M. Randić, *J. Chem. Inform. Comput. Sci.* **37**, 672 (1997).
- ⁶⁹S. N. Pozdnyakov, M. J. Willatt, A. P. Bartók, C. Ortner, G. Csányi, and M. Ceriotti, arXiv preprint arXiv:2001.11696 (2020).
- ⁷⁰O. A. von Lilienfeld, R. Ramakrishnan, M. Rupp, and A. Knoll, *Int. J. Quantum Chem.* **115**, 1084 (2015).
- ⁷¹R. Todeschini and V. Consonni, *Handbook of Molecular Descriptors*, edited by R. Mannhold, H. Kubinyi, and H. Timmerman, *Methods and Principles in Medicinal Chemistry*, Vol. 11 (Wiley-VCH, New York, 2000) p. 688.
- ⁷²J. Behler and M. Parrinello, *Phys. Rev. Lett.* **98**, 146401 (2007).
- ⁷³J. Behler, *J. Chem. Phys.* **134**, 074106 (2011).
- ⁷⁴E. A. Engel, A. Anelli, A. Hofstetter, F. Paruzzo, L. Emsley, and M. Ceriotti, *Phys. Chem. Chem. Phys.* **21**, 23385 (2019).
- ⁷⁵J. E. Moussa, *Phys. Rev. Lett.* **109**, 059801 (2012).
- ⁷⁶K. Hansen, F. Biegler, R. Ramakrishnan, W. Pronobis, O. A. von Lilienfeld, K.-R. Müller, and A. Tkatchenko, *J. Phys. Chem. Lett.* **6**, 2326 (2015).
- ⁷⁷B. Huang and O. A. von Lilienfeld, *J. Chem. Phys.* **145**, 161102 (2016).
- ⁷⁸W. Pronobis, A. Tkatchenko, and K.-R. Müller, *J. Chem. Theory Comput.* **14**, 2991 (2018).
- ⁷⁹R. Ditchfield, *Mol. Phys.* **27**, 789 (1974).
- ⁸⁰K. Wolinski, J. F. Hinton, and P. Pulay, *J. Am. Chem. Soc.* **112**, 8251 (1990).
- ⁸¹J. R. Cheeseman, G. W. Trucks, T. A. Keith, and M. J. Frisch, *J. Chem. Phys.* **104**, 5497 (1996).
- ⁸²M. J. Frisch, G. W. Trucks, H. B. Schlegel, G. E. Scuseria, M. A. Robb, J. R. Cheeseman, G. Scalmani, V. Barone, G. A. Petersson, H. Nakatsuji, *et al.*, Revision A **3** (2016).
- ⁸³J. J. Stewart, "Mopac2016," (2016), *stewart Computational Chemistry*, Colorado Springs, CO, USA, [HTTP://OpenMOPAC.net](http://OpenMOPAC.net).
- ⁸⁴J. Tomasi, B. Mennucci, and R. Cammi, *Chem. Rev.* **105**, 2999 (2005).
- ⁸⁵S. Chakraborty, P. Kayastha, and R. Ramakrishnan, *J. Chem. Phys.* **150**, 114106 (2019).
- ⁸⁶T. Fink and J.-L. Reymond, *J. Chem. Inf. Model.* **47**, 342 (2007).
- ⁸⁷L. C. Blum and J.-L. Reymond, *J. Am. Chem. Soc.* **131**, 8732 (2009).
- ⁸⁸L. C. Blum, R. van Deursen, and J.-L. Reymond, *J. Comput. Aided Mol. Des.* **25**, 637 (2011).
- ⁸⁹E. J. Corey, B. Czakó, and L. Kürti, *Molecules and Medicine* (John Wiley & Sons, 2007).
- ⁹⁰N. M. O'Boyle, M. Banck, C. A. James, C. Morley, T. Vandermeersch, and G. R. Hutchison, *J. Cheminformatics* **3**, 33 (2011).
- ⁹¹M. D. Hanwell, D. E. Curtis, D. C. Lonie, T. Vandermeersch, E. Zurek, and G. R. Hutchison, *J. Cheminformatics* **4**, 17 (2012).
- ⁹²T. A. Halgren, *J. Comput. Chem.* **17**, 490 (1996).
- ⁹³L. Himanen, M. O. J. Jäger, E. V. Morooka, F. Federici Canova, Y. S. Ranawat, D. Z. Gao, P. Rinke, and A. S. Foster, *Comput. Phys. Comm.* **247**, 106949 (2020).
- ⁹⁴A. S. Christensen, F. A. Faber, B. Huang, L. A. Bratholm, A. Tkatchenko, K.-R. Müller, and O. A. von Lilienfeld, "QML: A python toolkit for quantum machine learning," (2017), <https://github.com/qmlcode/qml>.
- ⁹⁵L. S. Blackford, J. Choi, A. Cleary, E. D'Azevedo, J. Demmel, I. Dhillon, J. Dongarra, S. Hammarling, G. Henry, A. Petitet, K. Stanley, D. Walker, and R. C. Whaley, *ScaLAPACK Users' Guide* (Society for Industrial and Applied Mathematics, Philadelphia, PA, 1997).
- ⁹⁶S. Krishnan, A. Ghosh, M. Gupta, P. Kayastha, S. Senthil, S. K. Das, S. C. Kandpal, S. Chakraborty, A. Gupta, and R. Ramakrishnan, "MolDis: A big data analytics platform for molecular discovery," (2020), <https://moldis.tifrh.res.in/>.
- ⁹⁷S. Molchanov and A. Gryff-Keller, *J. Phys. Chem. A* **121**, 9645 (2017).
- ⁹⁸M. F. Langer, A. Goeßmann, and M. Rupp, arXiv preprint arXiv:2003.12081 (2020).
- ⁹⁹D. Kilymis, A. P. Bartók, C. J. Pickard, A. C. Forse, and C. Merlet, *Phys. Chem. Chem. Phys.* (2020).